Rheometry and Polymorphism of Cocoa Butter During Crystallization Under Static and Stirring Conditions

Jorge F. Toro-Vazquez[a,*], David Pérez-Martínez[b], Elena Dibildox-Alvarado[a], Miriam Charó-Alonso[a], and Jaime Reyes-Hernández[b]

[a]Facultad de Ciencias Químicas, Universidad Autónoma de San Luis Potosí, San Luis Potosí, México, and [b]Programa de Posgrado en Alimentos del Centro Facultad de Química–Departamentode Investigación y Posgrado en Alimentos, Universidad Autónoma de Querétaro, Querétaro, México

ABSTRACT: In this work the association between polymorphism and the crystal network structure developed by the TAG of cocoa butter (CB) was investigated under static and stirring crystallization conditions using a dynamic mechanical spectrometer. The results obtained showed that parameters obtained through oscillatory rheometry (i.e., phase shift angle, δ) followed the polymorphism of CB during static crystallization. Although standard DSC was not capable of differentiating the α to β′ phase transformation from the direct β′ crystallization from CB melt, δ rheograms measured these two processes separately. Additionally, through oscillatory rheometry, we followed the dimensionality of the crystal network during CB crystallization. Within this context, the pre-exponential term (ln γ) from the weak-link regime equation for colloidal dispersions was much more sensitive than the fractal dimension (*D*) to differences in crystal size, spatial distribution of the crystal network, and melting temperature of the β′ phase of CB. On the other hand, torque measurements obtained during CB crystallization under stirring conditions showed a shear rate effect that favored TAG development in the β phase at temperatures of 19, 22, and 26.5°C, particularly at shear rates of 120 and 400 rpm. In contrast, under static conditions CB did not develop in the β phase at any of the crystallization temperatures investigated (i.e., 18 to 26.5°C).

Paper no. J10685 in *JAOCS 81,* 195–202 (February 2004).

KEY WORDS: Avrami index, cocoa butter, fractals, stirring crystallization.

Crystallization of cocoa butter (CB) provides unique characteristics of texture, mouth feel, and flavor release to chocolate and other confectionery products. Although CB is composed of various TAG, more than 75% exhibit a symmetrical conformation with oleic acid in the *sn*-2 position. Because of this homogeneity in TAG conformation and composition, polymorphism in CB is quite complex, i.e., at least six polymorphic forms have been observed. According to Wille and Lutton (1), each polymorph has a unique m.p. and crystal structural properties. These authors named the polymorphs from I to VI in increasing order of m.p. However, a study with real-time X-ray diffraction by van Malssen *et al.* (2) showed that forms III and IV according to the Wille and Lutton nomenclature exist as a range of β′ polymorphic phases rather than as two separate polymorphic phases. This property may be ascribed to cooperative interactions among the three major TAG of CB, i.e., StOSt, POSt, and POP, where St = stearate, O = oleate, and P = palmitate. Accordingly, TAG in CB crystallizes in the β′ phase as a distribution of crystallites with a particular TAG composition, providing a distribution of individual melting temperatures and diffraction patterns, all of them characteristic of the β′ polymorph (2).

CB is used as the main lipid phase in chocolate manufacture, but it is also used in combination with other vegetable oils, such as hydrogenated soybean oil and palm oil, in the elaboration of confectionery products. In any case, three major physical processes must be controlled when processing CB, namely, (i) crystallization of TAG, including in this size, shape, and polymorphic state of the crystals; (ii) development of the crystal network; and (iii) rheology of the chocolate mass or of the confectionary blend.

Several investigations have studied the effect of lipid composition and polymorphism on macroscopic properties of chocolate or confectionary products. However, the association of crystal network microstructure with macroscopic properties of CB and its products has seen limited investigation. Within this framework, the objective of this work was to follow, through rheological measurements, the polymorphism and crystal network structure developed by CB under static and stirring crystallization conditions.

MATERIALS AND METHODS

CB. One block (≈ 1000 g) of unrefined CB was obtained from a local distributor (PEALPAN, San Luis Potosí, México). The block was melted at 80°C and kept at this temperature for 20 min with constant agitation. The melted CB was vacuum-filtered through Whatman no. 5 paper and stored in amber flasks (250 mL) at 4°C under nitrogen.

Chemical analysis. The FA profile was analyzed by GC with a Shimadzu model GC-9A chromatograph with FID and a Supelco (Bellefonte, PA) fused-silica capillary column (30 m × 0.32 mm, 0.25 μm thickness; Omegawax 320). The analysis conditions were the following: column temperature 200°C, injector temperature 250°C, split 1:100, helium as carrier phase (110 kPa), and injection of 1 μL of prepared sample.

* To whom correspondence should be addressed at Facultad de Ciencias Químicas, Universidad Autónoma de San Luis Potosí, Av. Dr. Manuel Nava 6, Zona Universitaria, San Luis Potosí, SLP 78210, México.
E-mail: toro@uaslp.mx

Sample preparation, FA peak assignment, and quantification have been reported previously (3). The TAG profile was determined by HPLC using a Waters 1525 instrument (Waters Millipore Co., Milford, MA) with a light-scattering detector (Eurosep Instruments, Cergy Pontoise Cedex, France) and two Nova-Pak C_{18} columns (3.9 × 150 mm; Waters Millipore Co.) connected in series. Sample elution was carried out at room temperature using a solvent gradient of acetonitrile/dichloromethane from 70:30 to 30:70. The gradient program was applied in 1 h using two mixtures of acetonitrile/dichloromethane (90:10 and 10:90). The assignment of TAG peaks and their concentrations in CB were determined by the retention time of TAG standards (Supelco; Sigma Chemical Co., St. Louis, MO) and the development of calibration curves, respectively.

Rheometry studies under static conditions. A mechanical spectrometer (UDS 200; Physica, Stuttgart, Germany) with 50-mm diameter parallel-plate geometry (MP31; Physica) with a gap of 1 mm was used for measurements under static conditions. Temperature control was achieved by a Peltier system located in the base of the measurement geometry. This geometry has a well-defined mathematical model applicable even to nonhomogeneous systems such as a suspension of crystals in a liquid phase. This situation holds as long as the boundary conditions for the model are considered (i.e., measurements within the linear viscoelastic region). Thus, the melted CB (80°C) was applied on the base of the plate, avoiding the formation of bubbles, and the superior plate was positioned on the sample surface using the auto-gap function available in the rheometer software (Universal Software US 200; Physica). A temperature program was applied to CB as follows. First, the sample was held at 80°C for 20 min to erase the crystal memory, and then it was cooled at 20°C/min to 53°C; further cooling was continued at a rate of 1°C/min until the crystallization temperature was attained (i.e., 18, 18.5, 19, 20, 22, and 26.5°C). For each crystallization temperature (T_{Cr}) and for the different crystallization stages of CB, the linear viscoelastic region (LVR) of the system was established by using a constant angular frequency of 1 rad/s. With this information, oscillatory stress programs were developed with the rheometer software to apply a variable strain to the system, always within the LVR for the different crystallization stages at the different T_{Cr}. The strain interval applied, considering all T_{Cr} investigated and the different crystallization stages, varied from 0.025 up to 2.5% (0.01 to 1 mrad). The rheograms were obtained by plotting the storage modulus (G'), loss modulus (G''), or the phase shift angle (δ) of the crystallizing CB as a function of crystallization time.

Rheometry studies under stirring conditions. Rheological properties of two-phase systems (i.e., a crystallizing system) under stirring conditions may lead to incorrect measurements due to solid particle (i.e., crystals) sedimentation and their slip at the receptacle walls (4). Among the alternatives investigated to avoid such spurious flow phenomena is the use of mixing impellers. Such impellers provide torque data as a measurement of the flow resistance by the system against the rotational speed imposed by the impeller. Within this context, the helical ribbon geometry has yielded more stable torque and process viscosity measurements in suspension systems under stirring conditions than traditional geometries (4). Thus, a tailor-made stainless steel helical ribbon impeller, equipped with a sample container with circulating liquid jacket, was fitted to the mechanical spectrometer. The dimensions of the geometry of the impeller (Fig. 1) were the ones described by Brito-de la Fuente *et al.* (4). As recommended by these authors, during measurements the ratio of the height of the sample (i.e., melted CB = 3.78 cm) within the container to the height of the impeller (i.e., h = 3.15 cm in Fig. 1) was 1.20. The sample container included a jacket for temperature control, which was achieved by a constant-temperature bath (Brookfield TC-500; Brookfield Engineering Laboratories, Middleboro, MA) using a 50:50 mixture of ethylene glycol/distilled water. The bath provided an average cooling rate of 1.2°C/min. Process temperature during crystallization was measured by a high-precision thermopar located in the interior of the sample container (≈0.4 cm from the interior wall and ≈0.5 cm from the sample surface) and stored in a computer *via* a programmable temperature controller (Brookfield 107).

The T_{Cr} values evaluated under stirring conditions were 18, 19, 22, and 26.5°C. Additionally, at each T_{Cr} three stirring rates were tested (i.e., 1, 120, and 400 rpm), which were controlled by the software of the rheometer. Initially, 23 mL of melted CB (80°C) was added to the sample container and heated for 20 min at 80°C to erase crystal memory. Then the sample was cooled (≈1.2°C/min) at a given stirring rate until the T_{Cr} was attained. Torque measurements at a given T_{Cr} and stirring rate were obtained as a function of crystallization time.

Samples of the crystallizing CB were obtained at three different stages of crystallization, obtaining the melting thermo-

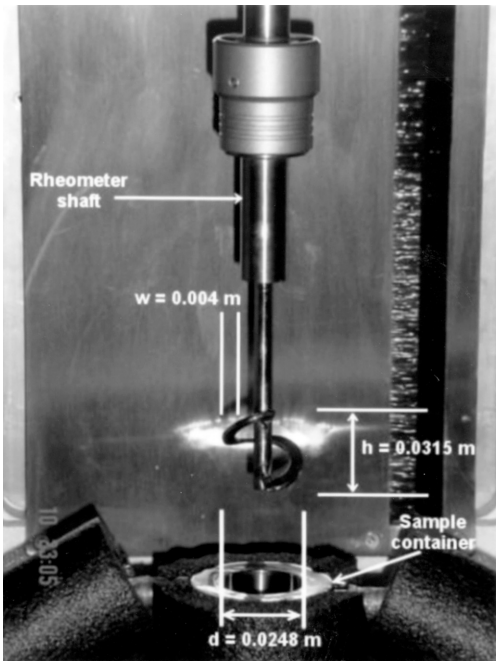

FIG. 1. Dimensions of the helical ribbon impeller used for rheological measurements under stirring conditions.

grams from T_{Cr} up to 80°C by DSC. However, in this manuscript we discuss only melting data of samples collected at the end of the crystallization.

DSC and Avrami index measurement. The isothermal crystallization thermograms were done in DSC equipment (DSC-7; PerkinElmer, Norwalk, CT) equipped with a dry box. The DSC was previously calibrated for temperature and heat involved in phase changes (melting/crystallization) as previously indicated (5). Empty aluminum pans were used as a reference. The sample of CB (≈8 mg) was sealed in an aluminum pan and held for 20 min at 80°C. Afterward, the system was cooled (20°C/min) to 53°C and held at this temperature for 2 min before continued cooling (1°C/min) to the T_{Cr} (18, 18.5, 19, 20, 22, and 26.5°C). After completion of the crystallization exotherm (i.e., heat capacity returned to the baseline), the system was left at the isothermal temperature for an additional 30 min. After this time the melting thermograms were determined at a heating rate of 5°C/min, calculating the melting temperature at the peak (T_p) of the endotherm using the first derivative of the heat flux as described previously (5). The difference in heat capacity between the reference and sample cells was partly compensated by using in the reference cell a sealed pan with the same weight of aluminum as CB in the sample pan (≈8 mg). The melting thermograms for samples of crystallizing CB under stirring conditions were done with the same procedure. However, in this case the melting temperature interval was from T_{Cr} up to 50°C.

On the other hand, in using the Avrami equation as described by Toro-Vazquez *et al.* (5), the fractional crystallization values *(F)* as a function of time and the Avrami index (*n)* were calculated from the crystallization exotherm of the relatively stable polymorph developed at the T_{Cr} investigated (i.e., β′).

In all cases at least two replicates (i.e., two independent determinations) were done.

Measurement of the fractal dimension. The measurement of the dimensionality of the TAG crystals network was based on the weak-link regime for colloidal dispersions (i.e., systems with a high volume fraction of solids) (6). In these systems G' increases as a function of the volume fraction of solid fat (ϕ) following Equations 1 and 2:

$$G' = \gamma\phi^m \quad [1]$$

$$\ln G' = \ln \gamma + m(\ln \phi) \quad [2]$$

$$m = 1/(3 - D) \quad [3]$$

where m depends on the mass fractal dimension (D, Eq. 3), and γ, the pre-exponential term, is a constant independent of ϕ but dependent on the size of the primary particles and on the interactions between them (i.e., polymorphic nature of the fat) (6).

Then, by assuming that the fractional crystallization values as a function of time (F from the Avrami equation) are equal to ϕ, plots of ln G' vs. ln F at each T_{Cr} are used to evaluate the development of the fractal organization during TAG crystallization in CB (Eq. 4), so long as both F and G' are measured at identical crystallization times. Thus, from ln G' vs. ln F curves, D and ln γ were calculated from the last linear slope and the corresponding intercept, respectively. Duplicate determinations were made and the mean and SD of D and ln γ calculated.

$$\ln G' = \ln \gamma + m \ln F \quad [4]$$

RESULTS AND DISCUSSION

The FA and TAG profiles of the CB used in this research are shown in Table 1. There were some discrepancies between the concentration of linoleic acid and arachidic acid found by GC compared with their TAG concentration determined by HPLC. Although the FID used in GC allows normalization of FA chromatogram areas according to the method of Ackman and Sipos (7), the light-scattering detector has a slight tendency to overestimate larger peaks compared with the smaller (8), owing to the nonlinearity of the detector response as function of TAG concentration (9). Since linoleic acid (Ln) and arachidic acid (A) are present in TAG that are found in low concentrations in CB (e.g., PLnO, StLnO, StOA, and the like), this might explain their lower concentration when determined by HPLC (i.e., linoleic acid 1.5% and arachidic acid 0.33%) in comparison with the value obtained by GC (Table 1). FFA, MAG, and DAG concentrations were not determined. The symmetrical saturated-unsaturated-saturated (SUS)-type TAG (i.e., StOSt, POSt, and POP) were ≈86%, the di-unsaturated asymmetrical TAG (i.e., POO and StOO) were ≈6.5%, and tri-saturated TAG (i.e., StStSt, PStSt, and PPSt) were ≈1.1% of the concentration. By using the concentration of these three TAG families, Chaiseri and Dimick (10) reported general differences among CB of six different origins. Such differences were associated with the nucleation behavior of CB, supporting its classification as rapid or slow nucleating. Thus, slow-nucleating CB showed a higher concentration of di-unsaturated asymmetrical TAG than rapid-nucleating CB.

TABLE 1
FA and TAG Concentration Profiles of Cocoa Butter

FA	Concentration[a] (%, w/w)	TAG	Concentration[b] (%, w/w)
M, myristic	0.1 (± 0.0)	PLnO	0.2 (± 0.1)
P, palmitic	25.8 (± 0.3)	PLnP	0.8 (± 0.2)
Po, palmitoleic	0.3 (± 0.0)	OOO	0.2 (± 0.1)
St, stearic	34.5 (± 0.2)	StLnO	0.2 (± 0.1)
O, oleic	34.9 (± 0.2)	POO	2.4 (± 0.4)
Ln, linoleic	3.0 (± 0.0)	PLnSt	2.1 (± 0.3)
Le, linolenic	0.2 (± 0.0)	POP	15.7 (± 0.5)
A, arachidic	1.0 (± 0.0)	StOO	4.1 (± 0.5)
Unidentified	0.2 (± 0.0)	StLnSt	1.2 (± 0.3)
		POSt	41.8 (± 2.6)
		PPSt	0.6 (± 0.3)
		StOSt	28.5 (± 0.8)
		PStSt	0.3 (± 0.2)
		StOA	1.0 (± 0.3)
		StStSt	0.2 (± 0.1)
		Unidentified	0.2 (± 0.1)

[a]Mean and SD of 10 independent determinations (n = 10).
[b]Mean and SD of eight independent determinations (n = 8).

In contrast, a higher concentration of symmetrical TAG was found in the rapid-nucleating CB (10). Following these criteria and by comparison with the TAG concentration profile reported by Chaiseri and Dimick (10), CB used in this investigation might be considered as slow-nucleating.

Figure 2 shows the thermograms of CB isothermally crystallized at 18, 18.5, 19, 20, and 22°C. The crystallization temperature of 26.5°C was included in this study based on the results of Davis and Dimick (11). Using absorbance measurements at 500 nm, these authors reported that at this T_{Cr} a seed crystal of high melting temperature (onset temperature of 72.4°C by DSC) is developed during early stages (e.g., 3 h) of static crystallization (11). However, with the CB used in this study, no particular crystallization exotherm was detected by DSC at T_{Cr} = 26.5°C even after 18 to 20 h. However, at T_{Cr} values between 18 and 20°C, the presence of two peaks was evident, and, given the crystallization conditions and the phase diagram for CB reported by van Malssen *et al.* (2), the first peak was assigned to the α polymorph, and the second to the β′ polymorph. The magnitude of the α polymorph peak decreased as the crystallization temperature increased, and at 22°C only a wide exotherm was observed. This exotherm corresponded to the β′ polymorph. This crystallization behavior agrees with the CB phase diagram developed by van Malssen *et al.* (2).

For data analysis each thermogram in Figure 2 was superimposed on the corresponding δ rheograms. Examples of such plots at 18.5, 19, and 22°C are shown in Figures 3 to 5. However, when using different equipment to follow crystallization, comparison between results must be done with caution. Differences in weight or volume of samples used, equipment design and its impact on the thermodynamics of the system, and heat and mass transfer conditions existing in each measurement device affect crystallization to a different extent. Such factors must be kept in mind when comparing crystallization data obtained with different equipment, such as when superimposing the DSC thermograms and rheological data shown in Figures 3–5 (5).

To understand the use of the δ rheograms, we must first clarify some concepts. The ratio between G' and G'' establishes

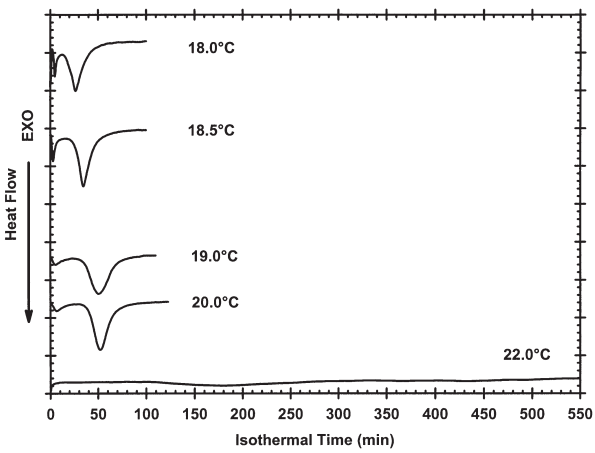

FIG. 2. Isothermal crystallization thermograms for cocoa butter at different crystallization temperatures.

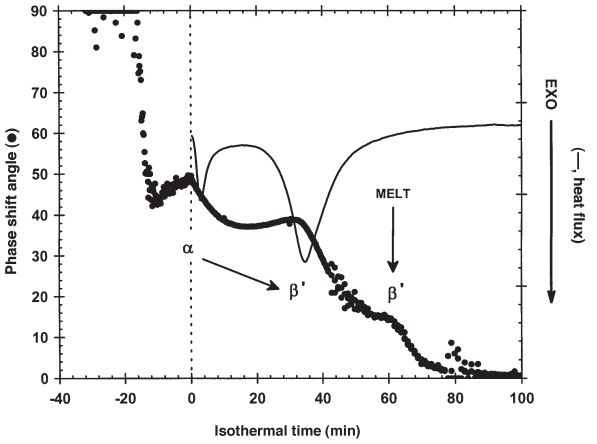

FIG. 3. Phase shift angle (δ) rheogram superimposed on the isothermal crystallization thermogram (18.5°C). The dotted line indicates the beginning of isothermal conditions. Polymorphic phases during crystallization as described in the text are shown.

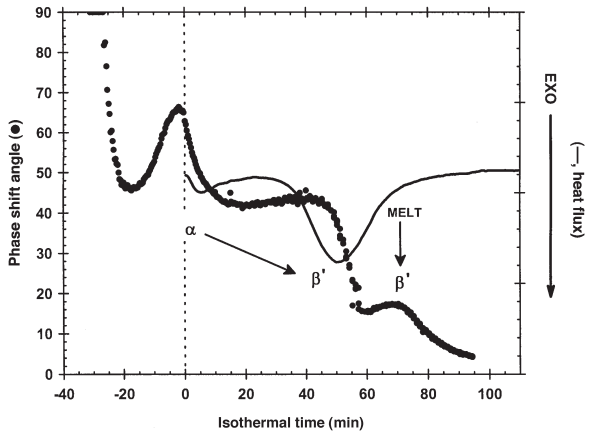

FIG. 4. Phase shift angle (δ) rheogram superimposed on the isothermal crystallization thermogram (19.0°C). The dotted line indicates the beginning of isothermal conditions. Polymorphic phases during crystallization as described in the text are shown.

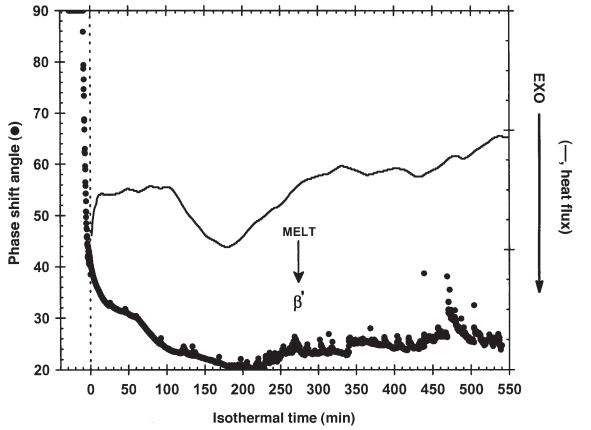

FIG. 5. Phase shift angle (δ) rheogram superimposed on the isothermal crystallization thermogram (22.0°C). The dotted line indicates the beginning of isothermal conditions. Polymorphic phases during crystallization as described in the text are shown.

changes in the viscoelastic properties of dispersed systems, such as the one studied here. The phase shift angle, δ, encompasses both parameters, evaluating in a quite sensitive way the viscoelastic changes of complex systems. Then, in a pure viscous system, such as a vegetable oil or completely melted CB, δ = 90°. Once TAG nucleation occurs, a drastic decrease in δ follows the phase change from liquid to solid. Eventually, if the system becomes fully crystallized, δ becomes zero. The heat released during the crystal growth process is shown in δ rheograms as a peak (5). In a previous study with palm stearin/sesame oil blends, we observed a single crystallization peak in both the thermograms and the rheograms (5). However, in this system just one polymorph was involved in crystallization. In contrast, in CB crystallization several polymorphs are involved, and both rheograms and thermograms were more complicated (Figs. 3–5). Additionally, at the low cooling rate and the crystallization temperatures used, a solid-like behavior was already developing in CB even before attaining isothermal conditions. This nucleation stage was established, giving the dramatic decrease in δ (from its original 90° value) that occurred during the cooling stage (Figs. 3–5). Similar behavior was observed in the crystallization of palm stearin/sesame oil blends at a cooling rate of 1°C/min (5). However, conclusions from this stage (i.e., variation of the crystallization onset as a function of T_{Cr}) must be done with caution since nonisothermal nucleation follows different kinetics from those under isothermal conditions. In contrast, previous research with palm stearin/sesame oil blends showed that under isothermal conditions the induction time for crystallization (i.e., nucleation), as measured by diffusive light scattering, was highly associated with the time δ decreased from its original 90° value (12). Under these crystallization conditions, both the induction time for crystallization by diffusive light scattering and the time where δ decreased from its original 90° value exhibited the same variation as a function of T_{Cr} (12).

As previously mentioned, at T_{Cr} values between 18 and 20°C, α was the earliest polymorph developed. Then the initial decrease observed in the δ rheograms and the first δ peak were associated with the nucleation and growth of the α crystals, respectively (Figs. 3 and 4). After this first δ peak occurring at T_{Cr} values between 18 and 20°C, a plateau followed, indicating no additional solid phase formation. Then a second δ peak occurred, which was immediately followed by additional solid phase formation (i.e., nucleation and crystal growth) as assessed by the further decrease in δ and the appearance of a third δ peak (Figs. 3 and 4). X-ray studies had shown that between 18 and 20°C just α and β′ polymorphs were developed (2); then the second δ peak must be associated with the development of β′ crystals. However, since at this stage no solid phase formation was evident, given the behavior of the δ profile, the second δ peak occurring at T_{Cr} values between 18 and 20°C was associated with the formation of β′ crystals through a solid-state transition from α (Figs. 3 and 4). Subsequently, the further decrease in δ and corresponding third δ peak must be associated with the nucleation and growth of additional β′ crystals. Such β′ crystals were developed directly from the melt through a facilitated nucleation mechanism. This mechanism occurred giving the β′ template previously developed in the system through the α to β′ solid-state polymorphic transition. Then, at T_{Cr} between 18 and 20°C, α crystals were developed early in the CB crystallization (first δ peak), which transformed into β′ through a solid-state transition (second δ peak). The presence of this β′ template facilitated the nucleation of additional β′ crystals, now directly from the CB melt (third δ peak).

As the crystallization temperature increased and lower amounts of α crystals were formed, as assessed by the magnitude of the first exotherm (Fig. 2), the corresponding rheograms became simpler. Finally, at 22°C, just one δ peak was observed (Fig. 5), corresponding with just one crystallization exotherm obtained at this temperature (Fig. 2). Since at 22°C no α state was developed (Fig. 2) and no α to β′ solid-state polymorphic transition occurred, β′ nucleation took longer because the only mechanism possible was direct nucleation from the CB melt.

Rheological data were used further to obtain the mass fractal dimension, D, and the pre-exponential term, ln γ. Representative plots of ln G' vs. ln F at T_{Cr} values of 18.5 and 19.0°C are shown in Figure 6. The ln G' vs. ln F curves described the evolution of the fractal organization as CB crystallization proceeded. The final dimensionality of the fractal crystal network

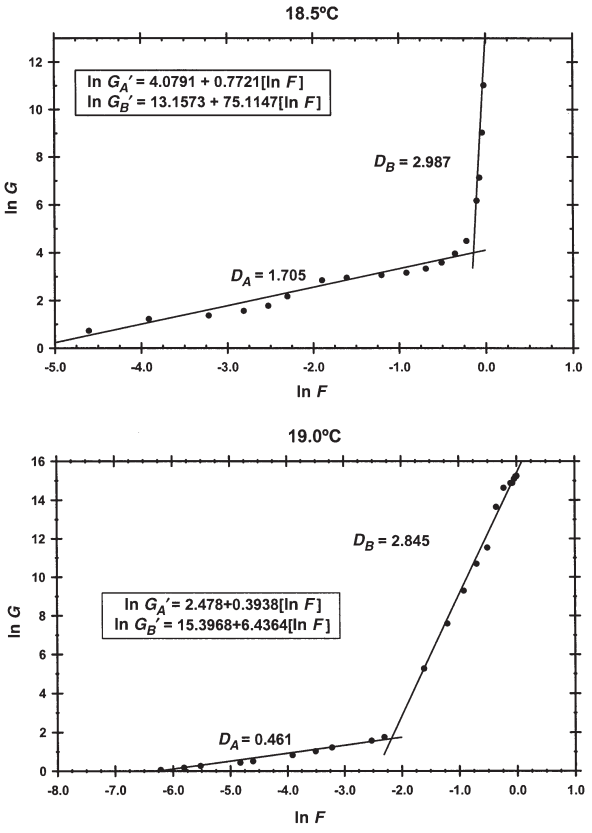

FIG. 6. Relationship between the storage modulus (G') and the fractional crystallization value (F) for cocoa butter isothermally crystallized under static conditions at 18.5 and 19.0°C. The linear regression fit for the two regions is shown along with the corresponding fractal dimension (D_A and D_B).

and the corresponding pre-exponential term for the different T_{Cr} values investigated are shown in Table 2, along with the values for the Avrami index (n) and the peak melting temperature (T_p). In accordance with van Malssen *et al.* (2), the β′ polymorph of CB crystallized as a phase range with different melting temperatures (Table 2), rather than a set of two individual melting phases as Wille and Lutton suggested (1), i.e., one for form III and another for form IV. Regarding the behavior of the n values, two different crystal growth mechanisms were observed at the T_{Cr} interval investigated. Thus, at crystallization temperatures greater than 19.0°C, n values were around 4.0, indicating a tri-dimensional (i.e., spherulitic) crystal growth mechanism. In contrast, at $T_{Cr} < 19.0$, TAG from CB followed a bi-dimensional (i.e., disk-like) crystal growth mechanism ($n \approx 3$). Similar behavior for n values in CB crystallization has been reported by McGauley and Marangoni (13). Several process variables affect the kinetics of crystallizing systems such as the one studied here. In particular, viscosity and supercooling play important roles during nucleation and crystal growth (14). Unfortunately, limited work has been done to understand the viscosity and supercooling interactions in determining the crystal growth process of TAG in complex systems (i.e., CB) (15). No particular relationship was observed between D and n, or ln γ and n. In fact, D remained constant at all crystallization temperatures investigated (Table 2). However, when ln γ was plotted as a function of T_{Cr}, two different zones were apparent (plots not shown), one with increasing ln γ values in a direct relationship with T_{Cr} (18–19°C), the other with the opposite behavior (Table 2) (20–22°C). Such zones provided crystals with quite different morphology as established by the polarized light microphotographs obtained at the end of the crystallization process (Fig. 7). The β′ polymorph crystallized *via* the α form developed a granular structure (Fig. 7 at 18 and 19°C), whereas at 20°C the clustering of spherulites was evident. This resulted in a completely different crystal structure and spatial distribution of the crystal network at $T_{Cr} = 20$°C from the ones obtained at T_{Cr} values ≤19°C (Fig. 7). McGauley and Marangoni (13) pointed out that in CB crystallized at 20°C, the α form becomes unstable

TABLE 2
Avrami Index (n), Fractal Dimension (D), Pre-exponential Term (ln γ), and Peak Melting Temperature (T_P) Values for Cocoa Butter Crystallized Under Isothermal Conditions at Different Crystallization Temperatures

Crystallization temperature (°C)	n (± SD)[a]	D (± SD)[a]	ln γ (± SD)[a]	T_P (± SD)[a] (°C)
18.0	3.47 (± 0.10)[b]	2.98 (± 5.4 x 10^{-4}) [b]	12.158 (± 0.54)[b]	27.8 (± 0.2)[b]
18.5	3.30 (± 0.32)[b]	2.99 (± 1.2 x 10^{-3})[b]	12.519 (± 0.90)[b]	27.8 (± 0.3)[b]
19.0	3.66 (± 0.33)[b,c]	2.91 (± 9.3 x 10^{-2})[b]	13.067 (± 3.29)[b]	27.5 (± 0.3)[b]
20.0	4.22 (± 0.47)[c]	2.99 (± 5.0 x 10^{-3})[b]	7.119 (± 3.83)[c]	28.1 (± 0.0)[c]
22.0	3.90 (± 0.20)[b,c]	2.96 (± 1.9 x 10^{-2})[b]	5.396 (± 0.94)[c]	29.5 (± 0.8)[c]

[a]Mean ± SD of at least two replicates. For each column, values with a different letter (b,c) are significantly different (LSD test, $P < 0.10$).

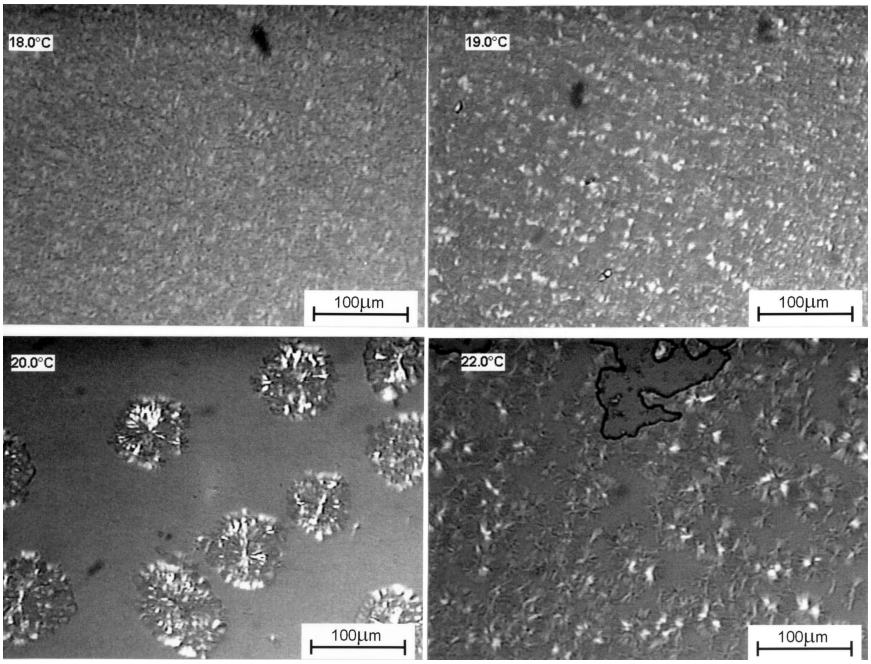

FIG. 7. Polarized light microphotographs of cocoa butter statically crystallized at 18.0, 19.0, 20, and 22°C.

and its polymorphic transformation toward β′ must be fast. At a T_{Cr} of 22°C, where β′ crystallizes directly from liquid CB, a somehow different morphology was observed with spherulites formed by needle-like structures (Fig. 7). Then similar D values were obtained by β′ crystals with different sizes, shapes, and melting temperatures (Table 2). In contrast, the magnitude of ln γ was quite sensitive to differences in size of the β′ crystals, to their spatial distribution in the crystal network, and to changes in the melting temperature (Table 2, Fig. 7).

With respect to the rheograms obtained under stirring conditions, in all cases torque measurements observed a slight and concomitant increment until a sudden increase occurred. This dramatic increment in the torque value was always associated with an increment in the temperature of the system (Figs. 8 and 9). The temperature increments occurred because of the crystallization heat, generated mainly during the crystal growth process (5). The temperature increment in the system was greater the higher the shear rate applied and the lower the T_{Cr}. Under these crystallization conditions, temperature control was a less efficient means to dissipate the heat generated. Consequently, the actual crystallization temperature was 1 to 3°C higher than the nominal T_{Cr}, resulting in melting of some CB crystals already developed as evaluated by the decrease in torque observed at this crystallization stage in the system (e.g., Fig. 8 at 120 and 400 rpm). At the lowest shear rate used (i.e., 1 rpm) a continuation of the crystallization process followed this partial melting, as assessed by the increase in torque of the crystallizing system. An apparent torque plateau followed this process (e.g., Fig. 8 at 1 rpm). However, this last torque increment (i.e., continuation of the crystallization process) was less evident the higher the T_{Cr}. In contrast, at higher shear rates (i.e., 120 and 400 rpm), after partial melting of CB crystals a torque plateau was obtained (Figs. 8 and 9).

Particular behavior occurred at T_{Cr} of 18 and 19°C at 400 rpm. These crystallization conditions provided the highest shear rate and supercooling extent and consequently provided better thermodynamic conditions for TAG nucleation. Thus, at the cooling rate used (≈1.2°C/min) and the shear rate of 400 rpm, TAG crystallization began even before attaining isothermal conditions (i.e., T_{Cr} = 18.0°C, data not shown) or just after achieving T_{Cr} (i.e., at T_{Cr} = 19.0°C, 400 rpm, Fig. 8). Particularly at 18°C, torque increased (i.e., crystallization started) even before achieving T_{Cr}, and the nominal T_{Cr} was never controlled (T_{Cr} was between 18.2 and 23.2°C, data not shown). At 19°C, torque increased at just 1.5 min after achieving T_{Cr} and a parallel 1.0°C temperature increment occurred, which was controlled after ≈3.0 min (Fig. 9 at 400 rpm). These observations show how only 1°C difference (i.e., T_{Cr} of 18°C vs. T_{Cr} of 19°C) at the same shear rate affects the thermodynamics of the system (i.e., temperature control) and, subsequently, its crystallization kinetics.

The corresponding melting temperatures (T_P) of the CB

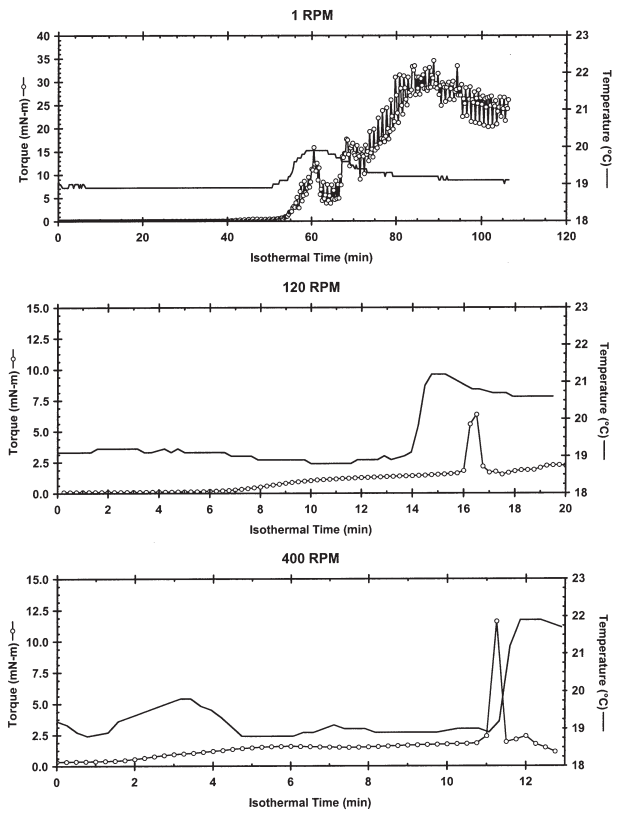

FIG. 8. Rheograms for cocoa butter crystallized at 19.0°C under stirring conditions at the shear rates indicated. The torque and process temperature values are shown.

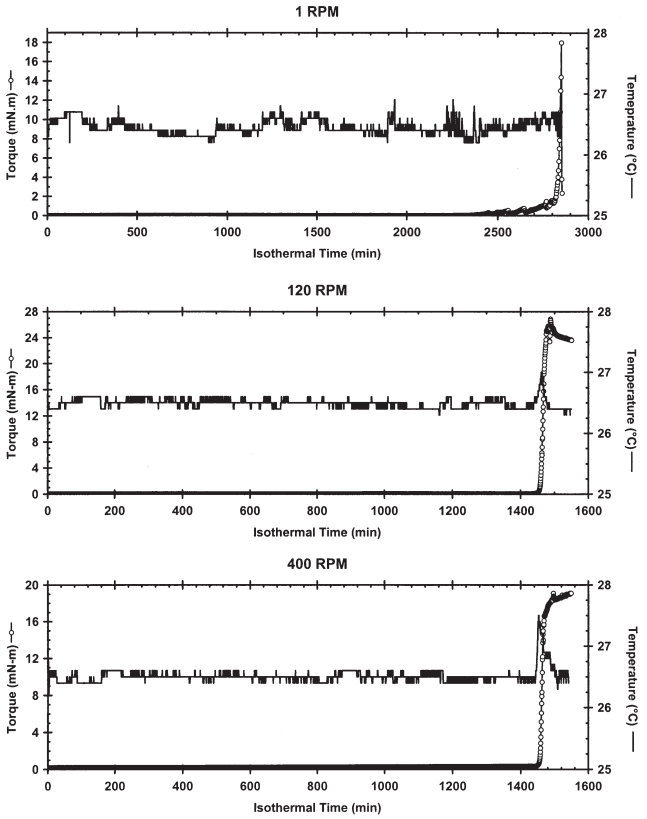

FIG. 9. Rheograms for cocoa butter crystallized at 26.5°C under stirring conditions at the shear rates indicated. The torque and process temperature values are shown.

crystals developed at the different shear rates and crystallization temperatures investigated are shown in Figure 10 in comparison with the ones obtained under static conditions. As pointed out previously in this paper, no particular crystallization exotherm was detected by DSC after 18 to 20 h of static crystallization at T_{Cr} = 26.5°C; subsequently, no T_P was reported. Within the crystallization temperature interval investigated, our data showed that at shear rates of 120 and 400 rpm, a T_p plateau was attained at T_{Cr} values between 22 and 26.5°C. Under such conditions, the mean T_p value was 32.6°C (± 0.7). This value is quite close to the X-ray diffraction melting temperature interval (29 to 34°C) determined by van Malssen (16) for the CB β phase. The development of this polymorphic state in CB might even occur through phase transformation at 400 rpm at a T_{Cr} of 19°C where the T_p value was 31.9°C (± 0.2°C).

In conclusion, oscillatory rheometry is used to describe and understand the crystallization process under static conditions. This work has shown that parameters obtained by oscillatory rheometry follow the polymorphism of CB during static crystallization. Our data suggest that standard DSC is not able to differentiate the α to β′ phase transformation and the β′ crystallization from the melt during CB crystallization. In contrast, δ rheograms measure these two processes separately. Oscillatory rheometry can be used to follow the development of the crystal network during CB crystallization. Within this context, the pre-exponential term (i.e., γ) proved to be a quite sensitive parameter to establish differences in crystal sizes, their spatial distribution in the network, and the melting temperature of the β′ phase of CB.

Torque measurements obtained during CB crystallization under stirring conditions do not provide information directly associated with structural characteristics of the crystals or crystal network properties. However, there is a shear rate effect that promotes the crystallization of CB in the β phase at lower temperatures compared with crystallization under static conditions. Shear rate may produce a hydrodynamic effect that favors TAG alignment and organization in the β phase.

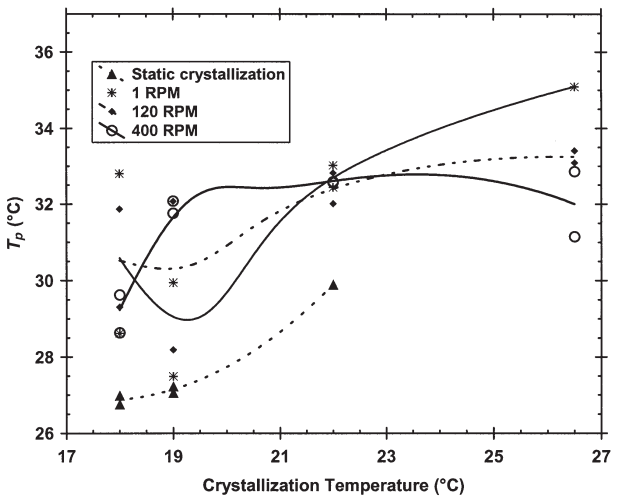

FIG. 10. Peak melting temperature (T_P) for the cocoa butter crystals developed at different crystallization temperatures under static and stirring conditions.

Additionally, the temperature increase observed during the massive crystallization stage might promote the β′ to β transition, since at this stage crystallization is taking place at a higher temperature than the nominal T_{Cr} and in the presence of crystals that withstand melting (i.e., β_1').

ACKNOWLEDGMENTS

The present research was supported by UASLP-FAI and CONACYT through grants C03-FAI-04-1920 and 2002-C01-39897, respectively.

REFERENCES

1. Wille, R.L., and E.S. Lutton, Polymorphism of Cocoa Butter, *J. Am. Oil Chem. Soc. 43*:491–496 (1966).
2. van Malssen, K., A. van Langevelde, R. Peschar, and H. Schenk, Phase Behavior and Extended Phase Scheme of Static Cocoa Butter Investigated with Real-Time X-ray Powder Diffraction, *Ibid. 76*:669–676 (1999).
3. Dibildox-Alvarado, E., and J. Toro-Vazquez, Isothermal Crystallization of Tripalmitin in Sesame Oil, *Ibid. 74*:69–76 (1997).
4. Brito-de la Fuente, E., J.A. Nava, L.M. López, L. Medina, G. Ascanio, and P.A. Tanguy, Process Viscometry of Complex Fluids and Suspensions with Helical Ribbon Agitators, *Can. J. Chem. Eng. 76*:689–695 (1998).
5. Toro-Vazquez, J.F., E. Dibildox-Alvarado, M. Charó-Alonso, V. Herrera-Coronado, and C.A. Gómez-Aldapa, The Avrami Index and the Fractal Dimension in Vegetable Oil Crystallization, *J. Am. Oil Chem. Soc. 79*:855–866 (2002).
6. Narine, S.S., and A.G. Marangoni, Fractal Nature of Fat Crystal Networks, *Phys. Rev. E 59*:1908–1920 (1999).
7. Ackman, R.G., and S.C. Sipos, Application of Specific Response Factor in the Gas Chromatographic Analysis of Methyl Ester of Fatty Acids with Flame-Ionization Detectors, *J. Am. Oil Chem. Soc. 41*:377 (1964).
8. Herslof, B., and G. Kindmark, HPLC of Triglycerides with Gradient Elution, *Lipids 20*:783–790 (1985).
9. Leray, C., *Separation and Quantification of Lipids by HPLC with Special Reference to Light-Scattering Detector*, Eurosep Instruments, Cergy St Christophe, France, 2001.
10. Chaiseri, S., and P.S. Dimick, Lipid and Hardness Characteristics of Cocoa Butter from Different Geographic Regions, *J. Am. Oil Chem. Soc. 66*:1771–1776 (1989).
11. Davis, T.R., and P.S. Dimick, Isolation and Thermal Characterization of High-Melting Seed Crystals Formed During Cocoa Butter Solidification, *Ibid. 66*:1488–1493 (1989).
12. Toro-Vazquez J.F., V. Herrera-Coronado, E. Dibildox-Alvarado, M. Charó-Alonso, and C. Gomez-Aldapa, Induction Time of Crystallization in Vegetable Oils, Comparative Measurements by Differential Scanning Calorimetry and Diffusive Light Scattering, *J. Food Sci. 67*:1057–1065 (2002).
13. McGauley, S.E., and A.G. Marangoni, Static Crystallization Behavior of Cocoa Butter and Its Relationship to Network Microstructure, in *Physical Properties of Lipids*, edited by A.G. Marangoni and S.S. Narine, Marcel Dekker, New York, 2002, pp. 85–123.
14. Hartel, R.W., *Crystallization in Foods*, Aspen, Gaithersburg, MD, 2001, pp. 192–232.
15. Toro-Vazquez, J.F., and E. Dibildox-Alvarado, Parameters That Determine Tripalmitin Crystallization in Sesame Oil, *J. Food Lipids 4*:269–282 (1997).
16. van Malssen, K.F., Real-Time X-Ray Powder Diffraction Applied to Cocoa Butter and Graphite Intercalates, Ph.D. Thesis, Universiteit van Amsterdam, The Netherlands, 1994.

[Received June 26, 2003; accepted November 12, 2003]